



THE UNIVERSITY *of* EDINBURGH

Edinburgh Research Explorer

A statistical framework to quantify spatial variation in channel gradients using the integral method of channel profile analysis

Citation for published version:

Mudd, SM, Attal, M, Milodowski, D, Grieve, SWD & Valters, DA 2014, 'A statistical framework to quantify spatial variation in channel gradients using the integral method of channel profile analysis', *Journal of Geophysical Research: Earth Surface*, vol. 119, no. 2, pp. 138–152. <https://doi.org/10.1002/2013JF002981>

Digital Object Identifier (DOI):

[10.1002/2013JF002981](https://doi.org/10.1002/2013JF002981)

Link:

[Link to publication record in Edinburgh Research Explorer](#)

Document Version:

Publisher's PDF, also known as Version of record

Published In:

Journal of Geophysical Research: Earth Surface

General rights

Copyright for the publications made accessible via the Edinburgh Research Explorer is retained by the author(s) and / or other copyright owners and it is a condition of accessing these publications that users recognise and abide by the legal requirements associated with these rights.

Take down policy

The University of Edinburgh has made every reasonable effort to ensure that Edinburgh Research Explorer content complies with UK legislation. If you believe that the public display of this file breaches copyright please contact openaccess@ed.ac.uk providing details, and we will remove access to the work immediately and investigate your claim.



A statistical framework to quantify spatial variation in channel gradients using the integral method of channel profile analysis

Simon M. Mudd,¹ Mikaël Attal,¹ David T. Milodowski,¹ Stuart W. D. Grieve,¹
and Declan A. Valters¹

Received 12 September 2013; revised 5 December 2013; accepted 6 December 2013.

[1] We present a statistical technique for analyzing longitudinal channel profiles. Our technique is based on the integral approach to channel analysis: Drainage area is integrated over flow distance to produce a transformed coordinate, χ , which has dimensions of length. Assuming that profile geometry is conditioned by the stream power law, defined as $E = KA^m S^n$ where E is erosion rate, K is erodibility, A is drainage area, S is channel gradient, and m and n are constants, the slope of a transformed profile in χ -elevation space should reflect the ratio of erosion rate to channel erodibility raised to a power $1/n$; this quantity is often referred to as the channel steepness and represents channel slope normalized for drainage area. Our technique tests all possible contiguous segments in the channel network to identify the most likely locations where channel steepness changes and also identifies the most likely m/n ratio. The technique identifies locations where either erodibility or erosion rates are most likely to be changing. Tests on a simulated landscape demonstrate that the technique can accurately retrieve both the m/n ratio and the correct number and location of segments eroding at different rates where model assumptions apply. Tests on natural landscapes illustrate how the method can distinguish between spurious channel convexities due to incorrect selection of the m/n ratio from those which are candidates for changing erodibility or erosion rates. We also show how, given erosion or uplift rate constraints, the method can be used to constrain the slope exponent, n .

Citation: Mudd, S. M., M. Attal, D. T. Milodowski, S. W. D. Grieve, and D. A. Valters (2014), A statistical framework to quantify spatial variation in channel gradients using the integral method of channel profile analysis, *J. Geophys. Res. Earth Surf.*, 119, doi:10.1002/2013JF002981.

1. Introduction

[2] Fluvial incision is one of the fundamental geomorphic processes that drive the evolution of eroding landscapes. Early geomorphologists recognized that channel gradients vary systematically with drainage area and reasoned that all else being equal, steeper channels should erode more rapidly [e.g., Davis, 1899]. This reasoning has motivated much research into bedrock rivers because it raises the possibility of using channel gradients to infer erosion rates. Howard and Kerby [1983] proposed that in bedrock rivers, erosion should be proportional to the power the river expends on its bed. Stream power depends on the flux of water in the channel, which is a function of drainage area, and the channel gradient. Thus, in areas of uniform lithology and climate a characteristic relationship between slope and drainage area can be expected for a given erosion rate. Later workers found that the geometry of bedrock river profiles is broadly consistent with a class of models similar to that first suggested by

Howard and Kerby [1983] and extended by others [e.g., Seidl and Dietrich, 1992; Howard, 1994]. Subsequently, so-called slope-area analysis has frequently been used to reveal patterns of erosion and, by inference, tectonic activity in channel networks [Stock and Montgomery, 1999; Kirby and Whipple, 2001; Kirby et al., 2003; Snyder et al., 2003; Wobus et al., 2006; Miller et al., 2007; DiBiase et al., 2010; Kirby and Ouimet, 2011; Kirby and Whipple, 2012].

[3] Topographic data are, however, inherently noisy. The noise arises from uncertainties in the data collection [e.g., Hodgson and Bresnahan, 2004; Eckert et al., 2005] but also from the natural heterogeneity that characterizes geomorphic systems: Channel beds are often uneven and local topographic features (e.g., steps in a river profile due to fractures in bedrock; accumulation of boulders at the base of a rock face) may not reflect regional erosion rates. Because slope is the spatial derivative of topography, slope data contain yet more noise, so analysis of channel slopes requires a degree of smoothing and data binning that may reveal broad patterns in the landscape [e.g., Wobus et al., 2006] but will fail to identify subtler spatial and/or temporal variations in erosion rates. Perron and Royden [2013], building on earlier work by Royden et al. [2000], offered an elegant solution to this problem by using an integral transformation of the river profile's horizontal coordinate into a variable χ (chi), which has units of distance but accounts for longitudinal variations

¹School of GeoSciences, University of Edinburgh, Edinburgh, UK.

Corresponding author: S. M. Mudd, School of GeoSciences, University of Edinburgh, Drummond St., Edinburgh EH8 9XP, UK. (simon.m.mudd@ed.ac.uk)

©2013. American Geophysical Union. All Rights Reserved.
2169-9003/14/10.1002/2013JF002981

in drainage area. Plots of channel elevations against this transformed length variable (or “chi plots;” *Perron and Royden* [2013]) can be used to reveal the steepness of river reaches without having to calculate channel slopes. This form of channel analysis, which *Perron and Royden* [2013] have called the integral method, has a number of attractive features. Critically, as the integral method does not involve differentiation, there is a significant reduction in noise relative to slope-area analysis. Consequently, estimates of channel steepness using the integral method have reduced uncertainty, and there is no longer a requirement to log-bin the data, which permits analysis of much finer details in the channel network (see *Perron and Royden* [2013] for a full discussion of the advantages and potential drawbacks of this method). The integral method has the potential to provide precise quantitative information about erosion rates and their spatial and temporal variations over areas for which topographic data are available, which could then be used to gain insight into the spatial and temporal variations in the controlling external forces, namely tectonics and climate. To achieve this, however, a transparent, robust, and objective method for discriminating between river reaches with different normalized steepness values must exist. In the following sections we (i) outline the theoretical principles of the integral method and discuss its application in steady state and transient and/or heterogeneous landscapes, (ii) develop a statistical framework with which to apply this method, and (iii) demonstrate the utility of this technique using a series of examples based on both numerical simulations and analysis of real landscapes.

2. The Integral Method of Channel Profile Analysis

[4] The evolution of a channel experiencing uplift and erosion driven by stream power can be stated as follows [e.g., *Howard and Kerby*, 1983; *Whipple and Tucker*, 1999]:

$$\frac{\partial z}{\partial t} = U(x, t) + K(x, t)A^m \left| \frac{\partial z}{\partial x} \right|^n, \quad (1)$$

where z (dimensions length; dimensions are hereafter denoted in brackets and abbreviated as [L]ength, [M]ass, and [T]ime) is the elevation of the channel, x [L] is a longitudinal coordinate, A [L²] is the drainage area, U [L T⁻¹] is the uplift rate, and K [T⁻¹ L^(1-2m)] is an erodibility coefficient which encapsulates the influence of climate, lithology, and other factors. The exponents m and n are empirically derived coefficients, although values of n have been proposed based on the mechanics of bedrock incision, ranging between 2/3 and 7/3 [*Whipple et al.*, 2000]. Both U and K may be functions of space and time, and K may also be a function of sediment supply [e.g., *Sklar and Dietrich*, 2004; *Cowie et al.*, 2008; *Hobley et al.*, 2011] and incorporate the influence of an erosion threshold and channel width adjustment [e.g., *Snyder et al.*, 2003; *Lague*, 2010; *Attal et al.*, 2011]. The stream power approach, its limitations, and alternatives are reviewed by *Lague* [2013]. The integral method devised by *Perron and Royden* [2013] (see also *Royden and Perron* [2013]) is based on the assumption that the evolution of the studied channels can be described by equation (1).

2.1. Chi Analysis: Steady State Example

[5] To introduce the integral method of channel analysis, we consider a simplified system in which K and U are constant in space and time, and uplift is balanced by erosion such that the elevation of the channel does not change in time (a so-called steady state channel):

$$\left| \frac{dz}{dx} \right| = \left(\frac{U}{K} \right)^{1/n} A(x)^{-m/n}. \quad (2)$$

[6] Equation (2) implies that plotting slope ($|dz/dx|$) against drainage area in log-log space should produce a straight line with a gradient $-m/n$ (often referred to as the channel concavity or concavity index, e.g., *Whipple and Tucker* [1999]), whereas the vertical position of the line in the plot should be indicative of the ratio of uplift to erodibility (U/K) raised to the power $1/n$. This relationship has been exploited by numerous authors to infer both erodibility [e.g., *Stock and Montgomery*, 1999] and tectonic uplift rates (see reviews by *Wobus et al.* [2006] and *Kirby and Whipple* [2012]). However, the noise inherent in slope data requires smoothing and averaging of slope-area data before they can be used to make inferences about erosion or tectonics [*Wobus et al.*, 2006]. In addition, slope-area data tend to show discontinuities, due to the fact that drainage area does not increase steadily downstream: Abrupt increases in drainage area at tributary junctions cause clustering of the data and create large uncertainties on regressions. An alternative approach is to avoid differentiation and thus eliminate the main source of noise [e.g., *Royden et al.*, 2000; *Pritchard et al.*, 2009; *Perron and Royden*, 2013]. One means of retaining drainage area and elevation information is to separate and then integrate equation (2) [e.g., *Royden et al.*, 2000; *Harkins et al.*, 2007; *Perron and Royden*, 2013]:

$$\int dz = \int \left(\frac{U}{KA^m} \right)^{1/n} dx. \quad (3)$$

[7] In a system in which K and U are constant in space and time, equation (3) may be integrated upstream from some base level at x_b to arrive at

$$z(x) = z(x_b) + \left(\frac{U}{KA_0^m} \right)^{1/n} \chi, \quad (4a)$$

where

$$\chi = \int_{x_b}^x \left(\frac{A_0}{A(x)} \right)^{m/n} dx, \quad (4b)$$

and A_0 is a reference drainage area, introduced to ensure the integrand in equation (4b) is dimensionless. The transformed coordinate, χ , has dimension of length and the elevation, $z(x)$, is a linear function of χ in this situation (K and U constant in space and time) according to equation (4a). Thus, a channel that obeys equation (2) will appear as a straight line in a chi plot, and the slope of the line will be a function of the uplift to erodibility ratio (U/K) raised to the power $1/n$. *Perron and Royden* [2013] pointed out several additional features that make chi plots an attractive alternative to slope-area plots. Importantly, the coordinate χ depends on the m/n ratio,

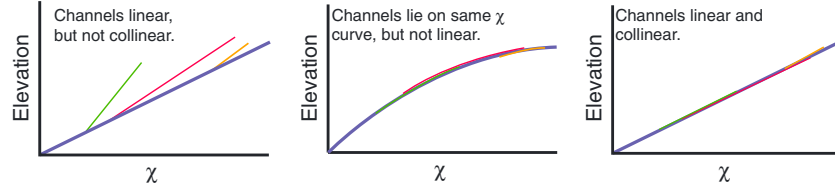


Figure 1. Sketch illustrating examples of linearity or nonlinearity of channels in χ -elevation space. Channel networks with spatially homogenous uplift and erodibility that are at steady state should have channels that are not just linear but collinear.

which is not known a priori but has been fixed in most slope-area analyses through the use of a reference concavity index: A value of 0.45–0.5 is frequently used, representing the concavity that river profiles should theoretically achieve should erosion rates be proportional to the specific stream power or shear stress [e.g., *Wobus et al.*, 2006]. However, *Perron and Royden* [2013] proposed two independent criteria to estimate and test the most likely m/n ratio for a steady state channel experiencing uniform uplift and incising rocks with uniform erodibility (equation (2)): (i) individual channels in the network should be linear in χ -elevation space and (ii) all channels in the network should be collinear in χ -elevation space (Figure 1). Therefore, the best fitting m/n value can be found by iterating through a range of m/n values and maximizing the R^2 value of the elevation data in χ space for the main stem channel and then for its tributaries.

2.2. Chi Plots in Transient and Spatially Heterogeneous Landscapes

[8] *Royden and Perron* [2013] demonstrated that chi plots could be used to analyze steady state channels in landscapes characterized by uniform uplift and erodibility, both spatially and temporally. They demonstrated further that the coordinate transformation of equation (4b) can be used to find families of analytical solutions for transient channel behavior. Using these solutions, *Royden and Perron* [2013] demonstrated the presence of what they termed “slope patches,” which are mathematical entities that migrate upstream in χ -elevation space. If $n = 1$, slope patches move upstream in χ space at a fixed rate, regardless of the uplift rate, and the χ -elevation plot is composed entirely of linear segments (Figure 2). If $n > 1$, slope patches move quicker if they are generated by an increase in uplift rate; if $n < 1$ slope patches generated by a decrease in uplift rate move faster. This behavior is consistent with theoretical work [*Rosenbloom and Anderson*, 1994; *Weissel and Seidl*, 1998; *Tucker and Whipple*, 2002] which showed that in river systems obeying equation (2), the celerity (C) of perturbations migrating up the channel is

$$C = KA^m S^{n-1}. \quad (5)$$

[9] For $n = 1$, the celerity of perturbation is independent of slope (and thus of uplift rate); if $n > 1$, the celerity of the perturbation is greater on steeper slopes and vice versa. When $n \neq 1$ there exists a possibility that an upstream slope patch may move faster than its downstream neighbor, resulting in nonlinear sections *Royden and Perron* [2013] termed

“stretch zones.” In addition, when $n \neq 1$ downstream patches may move quicker than upstream patches leading to a loss of information along the channel network; *Royden and Perron* [2013] termed these entities “consuming knickpoints.” In the case of time invariant but spatially varying uplift, *Royden and Perron* [2013] demonstrated that transformed channel profiles are made up of piecewise linear segments which reflect local uplift rates.

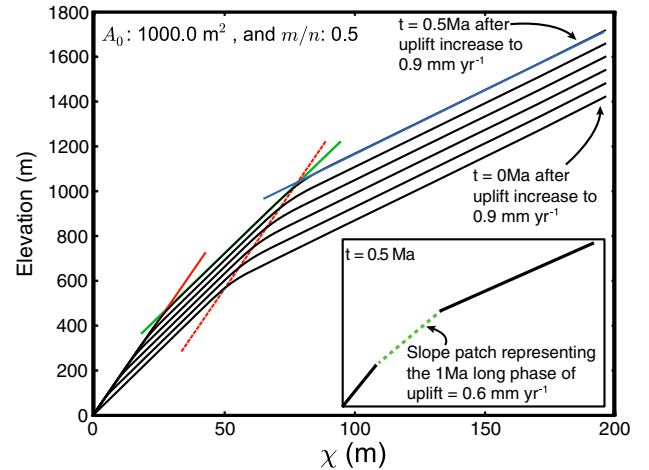


Figure 2. Illustration of upstream migration of channel segments in χ -elevation space. Profiles generated using the CHILD model (see text) with $n = 1$. A channel in steady state with an uplift rate of 0.3 mm yr^{-1} experiences two consecutive step increases in uplift rate 1 Ma apart, to 0.6 and then 0.9 mm yr^{-1} . The black curves show chi profiles at the time of the second step change and every 0.1 Ma thereafter. The blue, green, and red lines are parallel to portions of the channel adjusted to the different uplift rates 0.3 , 0.6 , and 0.9 mm yr^{-1} , respectively. The dashed red line is parallel to the solid red line: It is drawn to illustrate how a line crossing the intersection of the segments formed by uplift rates of 0.6 and 0.3 mm yr^{-1} is parallel to the segment formed by an uplift rate of 0.9 mm yr^{-1} . This demonstrates that when $n = 1$, channel segments representing a given phase during which external forcing was constant (or “slope patches,” see schematic chi plot in inset) maintain a constant length and slope in χ -elevation space. When n does not equal to 1, information can be lost as segments consume other segments, but as long as segments are not “erased,” they will retain some steepness information that can, in principle, be related to the uplift rates or climatic conditions under which they formed.

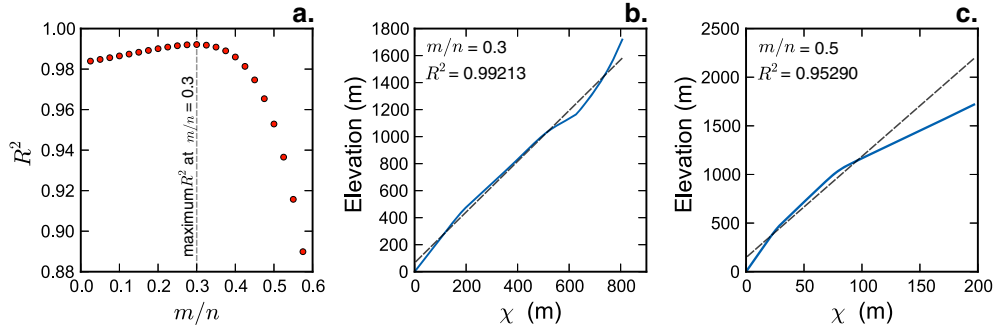


Figure 3. (a) Plot shows the R^2 values of a linear fit to channel data generated by the transient simulation described in Figure 2 as a function of the m/n ratio. (b) Plot shows the profile in χ -elevation space with an m/n ratio of 0.3, which has the highest R^2 for a linear fit to the channel data. (c) The true m/n is 0.5, and the χ -elevation profile for this m/n ratio is shown.

2.3. Need for a Statistical Approach to Create Chi Plots From Topographic Data

[10] To construct chi plots, the m/n ratio must be assigned. *Perron and Royden* [2013] suggest performing linear regression for a range of m/n ratios and selecting the ratio with the minimum value of R^2 . However, as discussed in the previous section, the results of *Royden and Perron* [2013] imply that, in transient landscapes, spatial or temporal changes in uplift rates could lead to channel profiles that are piecewise linear. This hinders attempts to find the most likely m/n value. For example, a channel that has undergone stepwise increases in uplift rates will be composed of two or more segments and will thus appear convex up (with a low R^2 value) in the chi plot with the true m/n ratio (Figure 3). *Perron and Royden* [2013] also suggested that in simple transient cases the collinearity of tributaries can be used to identify the correct m/n ratio, highlighting the need for statistical tests that go beyond minimization of an R^2 value. Thus, if our aim is to identify slope patches that are indicative of spatial or temporal changes in boundary conditions (uplift or climate) or rock properties, we need an objective, statistically robust, and reproducible method for doing so. In this contribution we present one such method.

3. A Statistical Method to Identify the Most Likely Combination of Segments in χ -Elevation Space

[11] The method begins with a channel network for which elevation (z), flow distance (x), and drainage area (A) have been extracted. Our approach tests every possible combination of linear channel segments to find the most likely m/n ratio and the most likely piecewise linear fit to channel profile data in χ -elevation space.

3.1. Integration of the Channel Profile

[12] The first step is to calculate the χ coordinate by integrating equation (4b) for each node in the channel network. For integration, we use the rectangle rule because increases in drainage area are focused at tributary junctions; the rectangle rule better captures the stepped nature of changes in drainage area along channels than other methods such as the trapezoid rule.

3.2. Segment Fitting Algorithm

[13] Our method relies on an algorithm that separates data into the most likely combination of piecewise linear segments.

We favor a technique that uses piecewise fitting over other approaches such as spline fitting [e.g., *Hansen and Kooperberg*, 2002], which joins segments that share end nodes, otherwise called “knots.” We do not tie segments because we want a technique that can capture the two types of knickpoints described by *Kirby and Whipple* [2012] as “vertical step” knickpoints, where there is a step between adjacent nodes in the channel network, as well as those they describe as “slope break” knickpoints where channel steepness differs above and below the knickpoint.

3.2.1. Partitioning the Data

[14] The first step in the segment fitting algorithm is to “partition” the data. Partitioning involves finding every combination of positive integers that sum to some integer N (e.g., 5 can be partitioned as 5; 4 + 1; 3 + 2; and 3 + 1 + 1). In our application, N is the number of nodes in χ -elevation space that we use for a particular channel, channel segment, or channel network. We use the partitioning algorithm described in *Skiena* [1990] and implemented by Frank Ruskey (<http://theory.cs.uvic.ca/inf/num/NumPartition.html>). To allow the user to define a minimum number of nodes in a segment, we have modified the *Skiena* [1990] algorithm to reject partitions that have less than the minimum number of nodes. The user is allowed to select a minimum number of nodes in a segment because we reason that allowing segments made up of two nodes, while always resulting in a perfect fit, will not be useful in reconstructing channel dynamics. We explore the sensitivity of results to the minimum segment length in sections 4.1 and 4.3.

[15] The partition function, often denoted by $P(N)$, describes how many partitions there are for a given integer N . This function is highly nonlinear. Example values of $P(N)$ are $P(10) = 42$; $P(100) = 190,569,292$; $P(200) = 397,299,029,388$ [*Andrews*, 1998]. The nonlinearity of the partition function precludes analysis of more than a few hundred nodes due to computational expense. We address this impediment to sampling every node in the network by using a Monte-Carlo sampling approach; each iteration samples a subset of nodes at reduced computational expense. This procedure is repeated until all nodes are sampled multiple times (section 3.2.2).

[16] Partitioning alone does not sample all possible channel segments, because segments could be arranged in different orders. Consider a channel with five nodes, further constrained by a minimum segment length of two; the possible partitions are therefore 5 and 3 + 2; however, the possible segment

combinations are 5, 3 + 2, and 2 + 3. We therefore permute all partitions to sample all possible segment combinations.

[17] A linear regression is performed on each segment. The slope, intercept, residuals, and R^2 of each segment are stored. *Royden and Perron* [2013] showed that under certain conditions (e.g., transience caused by changes in uplift rate with $n \neq 1$), linear segments of the channel profile in the chi plot will be connected by nonlinear segments (or “stretch zones”). Rather than performing both a linear and nonlinear fit on every segment, we perform only a linear fit. The rationale for this is that (i) we do not wish to overconstrain the fit, (ii) selecting the incorrect m/n ratio results in nonlinear sections in χ -elevation space, and we do not wish to “reward” nonlinearity as this could lead to poor constraints on the m/n ratio, and (iii) there is a simple relationship between the linear segments’ slope and erosion rate in χ -elevation space which does not apply in the stretch zones [see *Royden and Perron*, 2013, equation (16)].

[18] As the number of nodes in the channel grows, there is an ever increasing likelihood that some segments will be sampled more than once. For example, consider a channel with nine nodes and a minimum segment length of three. The partitions would then be 9; 6 + 3; 5 + 4; and 3 + 3 + 3. The segment starting on the first node and ending on the third node will be used in the partition 3 + 6 as well as the partition 3 + 3 + 3. To reduce computational expense, we precede partitioning by regressing all segments and storing the slope, intercept, R^2 , and a maximum likelihood estimator (MLE) of the regressed χ -elevation data in sparse matrices where the row represents the starting node of the segment and the column represents the finishing node of the segment.

3.2.2. Determining the Most Likely Combination of Segments

[19] The partition algorithm finds every possible combination of segment lengths, and permuting through these segment lengths results in every possible combination of segments along a thinned channel network. Because the partition function is highly nonlinear, it is necessary to limit the number of nodes considered by the segment fitting algorithm. The algorithm allows the user to select the maximum number of nodes to be analyzed in any given iteration of the segment fitting algorithm. Whereas partitioning 100 nodes requires 10^9 linear regressions, partitioning 200 nodes requires $\sim 10^{12}$ regressions. Beyond 200 nodes the computational expense is prohibitive; we recommend setting the maximum number of nodes (or “target nodes”) to 80–150. This creates a problem of resolution however because, in high-resolution data, channels may be made of more than 150 nodes; furthermore, we want to avoid a situation in which the resolution of the analysis depends on the number of nodes in the channels. We address this through an iterative approach which, for computational efficiency, samples a subset of data in each iteration but through iterations samples every data point in the channel network.

[20] We use what we call a “skipping” algorithm to select a subset of nodes from a data set. First, the number of nodes in the data set is compared to the target nodes to determine the mean number of nodes that must be “skipped” between two selected nodes to retain the correct number of target nodes in the thinned data set. For example, if the data set has 300 nodes and target nodes = 100, then for every node retained, the algorithm will skip two nodes. Skipping of data, however, is done probabilistically, although the first and last

nodes are always selected. After a node is selected, the code selects the next number of nodes to skip from a uniform distribution centered on the mean skip value with a range twice the mean skip value; for example, if the mean skip value is 2, skip values will be chosen in the range 0 to 4.

[21] The skip interval is determined by the number of nodes in the data set, but the user selects a “target skip” value which is the final resolution of the data at which the user wants to perform the analysis. Our iterative approach breaks the data set into smaller and smaller pieces until the mean skip (determined by dividing the number of data nodes by the number of target nodes) matches that of the target skip value.

[22] To iterate to the target skip value, all the data are thinned using the probabilistic skipping algorithm, and these data are then passed to the segment fitting algorithm. The fitting algorithm then determines the most likely segments for the data and returns the segment number associated with each node (Figure 4). This is recorded for each node in the analysis, and the process is repeated. Because the skipping algorithm is probabilistic, a different subset of nodes is analyzed in each iteration. After many iterations, each node will be associated with a data set comprising the number of the segment to which it will have been attributed in each iteration (Figure 4). The mean of these numbers is then calculated for each node. For nodes that lie unambiguously in a particular segment (for example, the first node is always in the first segment), the mean segment number will be an integer. Between unambiguous segments lie noninteger mean segment numbers. If the mean skip is greater than the target skip, the data are “broken” at natural segment breaks at nodes nearest to half an integer value (i.e., 1.5, 2.5, and 3.5). After breaking the data, each smaller data set is passed back to the segment fitting algorithm. This process is repeated until all of the “breaks” are analyzed at the resolution determined by the user-defined target skip value.

[23] Because a probabilistic approach is used to select data nodes repeatedly, each node records the slope and intercept of the segments in χ -elevation space, as well as the segment number and R^2 value. The mean and standard deviation of these data for each node is then calculated. Of these, the slope in χ -elevation space, which we call M_χ , is perhaps the most useful because it is related to the ratio between erosion rate (E) and erodibility (K):

$$M_\chi = \left(\frac{E}{KA_0^m} \right)^{1/n}. \quad (6)$$

[24] The intercept in χ -elevation space, which we call B_χ , can be used to identify steps in the channel network (e.g., segments that have the same M_χ but are separated by a vertical waterfall). Thus, by constraining both M_χ and B_χ we are able to identify two types of knickpoints: a change in B_χ with no change in M_χ above and below the knickpoint indicates a vertical step knickpoint, whereas a change in M_χ reveals a slope break knickpoint.

[25] The next step is to calculate an MLE for each segment:

$$\text{MLE} = \prod_{i=1}^N \frac{1}{\sqrt{2\pi}\sigma} \exp \left[-\frac{(r_i)^2}{2\sigma^2} \right], \quad (7)$$

where σ [L] is the standard deviation of the measured elevations. Many topographic data sets contain metadata

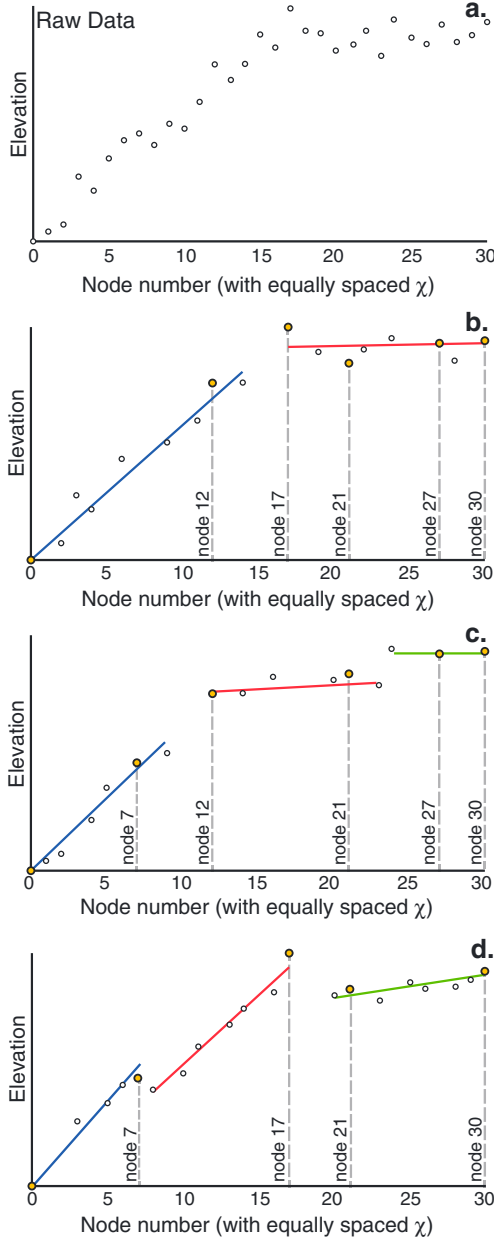


Figure 4. Cartoon depicting the skipping process and the selection of segment numbers. (a) A hypothetical data set with 31 data points is shown. (b–d) Plots show data after skipping. In this case the mean skip = 1, so skip values are randomly selected between 0, 1, and 2. In this hypothetical example, there are three iterations of the skipping algorithm. We highlight several nodes with yellow dots. Node 0 and node 7 are always in the first segment, so the mean segment number of these nodes will be = 1. The mean segment number of node 12 will be 1.5 since it is in segment 1 in the first iteration and segment 2 in the second iteration. Node 17 has an integer mean segment number, whereas nodes 21, 27, and 30 all have noninteger mean segment numbers.

describing the uncertainty of the elevations, which can guide the choice of σ . However, we also suggest considering “geomorphic noise,” that is, variation in the channel profile due to heterogeneity on scales of meters to tens of meters

(i.e., fracture patterns in rocks, bedrock sedimentary bedding, and boulders in the channel) that adds roughness to the channel profile and clouds the landscape-scale geometry of the river profile which is indicative of regional tectonics, lithology, or climate. The choice of σ will therefore depend on the application, and it is therefore crucial that users of the software report the value of this parameter. In section 4.1 we report on how much of an impact changing the value of σ can have on the number of segments selected by the software. Note that the MLE is multiplicative so that its value for a sequence of segments will be the product of the MLE of the individual segments.

[26] For a fixed number of segments, the most likely combination of these segments simply has the lowest MLE value. However, increasing the number of segments always results in a higher likelihood. Using the MLE alone is thus insufficient to differentiate models with different numbers of segments.

[27] An established statistical method for selecting a model that balances goodness of fit against model complexity is the Akaike Information Criterion (AIC) [Akaike, 1974]:

$$\text{AIC} = 2k - 2 \ln(\text{MLE}), \quad (8)$$

where k is the number of parameters. Each linear segment has two parameters, the slope of the line and its intercept, so $k = 2s$ where s is the number of segments. The model with the minimum value of the AIC is deemed the best model. Burnham and Anderson [2002] suggest that a correction should be made to the AIC if there are a finite number of samples; we therefore employ a corrected AICc [Hurvich and Tsai, 1989] to select the best model:

$$\text{AICc} = \text{AIC} + \frac{2k(k+1)}{N-k-1}, \quad (9)$$

where N is the sample size, or in this case the number of channel nodes used in the analysis. The AICc penalizes over fitting in small data sets, and Burnham and Anderson [2002, p. 445] suggest using AICc when $N/k < 40$. Because of the restriction on the number of nodes due to the computational expense of partitioning, almost any fitting of χ -elevation data will meet this criterion, and AIC converges to AICc when N is large so in the rare instances when the criterion fails (i.e., $N/k > 40$) AICc and AIC will take similar values. Thus, there is little reason to risk biasing the result by using the AIC rather than AICc. Figure 5 illustrates this partitioning process. We do not penalize segments whose fitted downstream node is lower than the elevation of the fitted upstream node; this is because if sections are connected by stretch zones, a linear fit to a nonlinear stretch zone can result in segments that do not always exhibit end nodes of monotonically increasing elevations.

[28] The choice of standard deviation (σ) in equation (7) will affect the output of the fitting algorithm. For a fixed number of segments, the most likely segments will always be the same, regardless of the value of σ . That is, the numeric value of the MLE will change but the most likely combination will not. Modifying the numeric value of the MLE, however, changes the second term of equation (8) but does not affect the first term of this equation. The result is that greater

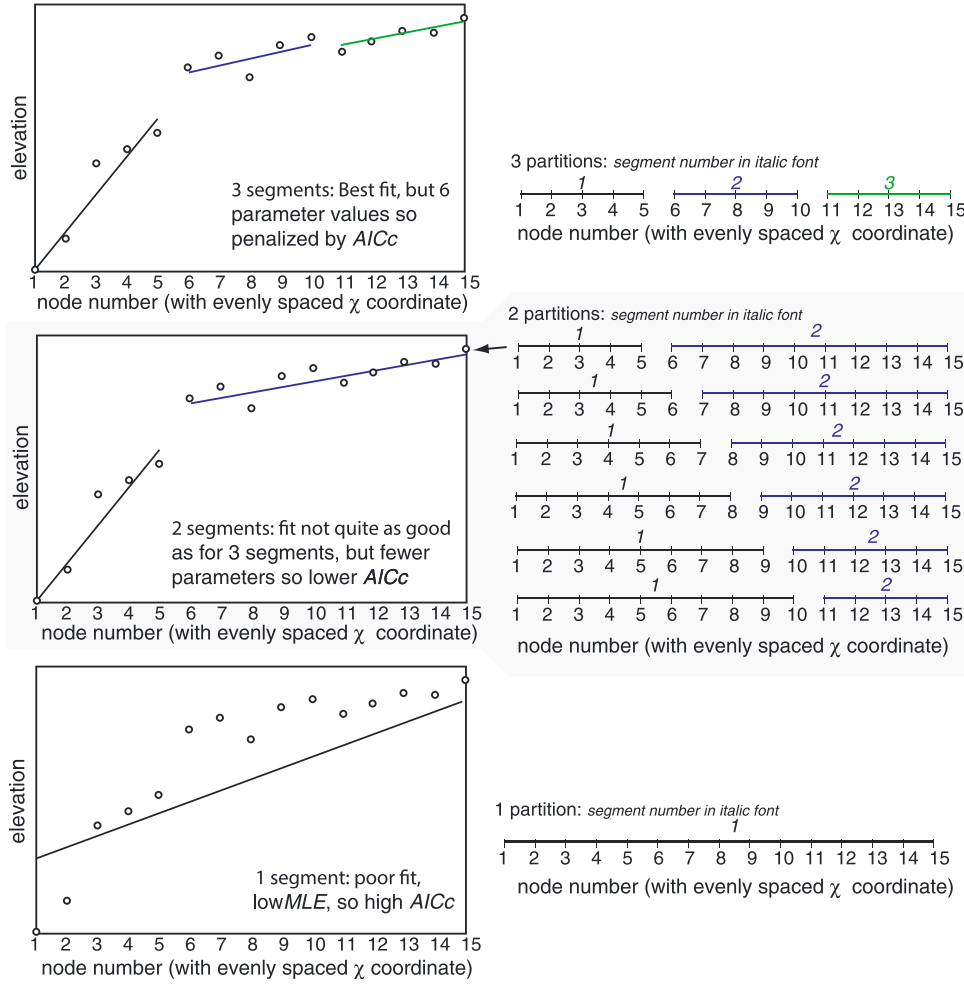


Figure 5. Illustration of the partitioning process (minimum partition length = five nodes in this case).

values of σ result in greater “penalties” for extra segments and in general the lower the value of σ , the more segments will be selected.

3.3. Selection of the m/n Ratio

[29] To differentiate between profiles generated using different m/n ratios, we use the MLE and $AICc$ information. Again, the MLE is not sufficient to discriminate fitted channel segments against each other because different m/n ratios may generate different numbers of best fit segments. We therefore store the cumulative $AICc$ values for all m/n values. The m/n ratio that produces the minimum cumulative $AICc$ value is considered the most likely. We perform two tests to determine the most likely m/n ratio: a collinearity test and a test for individual channels.

[30] In the collinearity test, the data from the entire channel network are pooled. This pooled data set undergoes the breaking processes described in section 3.2.2, but the $AICc$ values reported are cumulative for all the data rather than on a channel by channel basis. Our testing based on numerical simulations (see section 4.1) indicates this test can better identify the m/n ratio when analyzing data based on numerical simulations. Our tests on channels in natural environments (e.g., section 4.2) indicate however that there can be pitfalls to this method. If a tributary is hanging, for example, the data from this tributary will be lying above the main

stem’s data in χ -elevation space (by definition); because the algorithm will seek the m/n value that best superimposes data from the tributary and the main stem, the collinearity test may give spurious results for the best fit m/n ratio.

[31] The second test calculates the cumulative value of the $AICc$ for each individual channel. In this analysis, all tributaries are extended from their source to the drainage outlet. The rationale for this is that transient signals of uplift rate are translated through the channel network with celerity proportional to drainage area (see equation (5)) [Whipple and Tucker, 1999]. This means that any upstream propagation of uplift signals will slow down significantly as it enters small tributaries: steepened reaches in small tributaries will consequently often have limited spatial extent. The result is that if tributary channels are extended only to the junction with the main stem, the algorithm will not be able to find the short transient segment. The segment can be found, however, if the analyzed channel data include the tributary data and the main stem data downstream of the confluence.

[32] As described in section 3.2.2, the mean $AICc$ values are a result of many iterations of the segment fitting algorithm. The code also returns the standard deviation of the $AICc$ values for each m/n ratio, for the cumulative data (used in the collinearity test), and for each individual channel. The variability is due to the algorithm being performed on a different subset of data, chosen at random by the skipping algorithm,

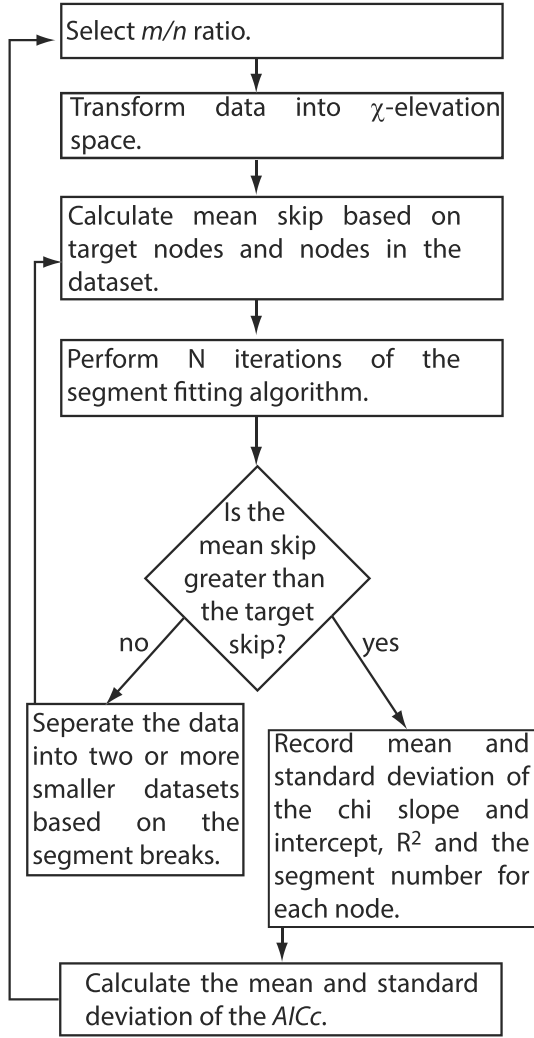


Figure 6. Flowchart for the segment fitting algorithm.

during individual iterations. The most likely m/n ratio is that with the minimum AICc value, but the standard deviation of the AICc values can be used to infer the range of plausible m/n values for the channel network. We recommend that authors interpret the m/n ratios with AICc values that are within 1 standard deviation of the minimum AICc values as being “plausible.” Figure 6 shows a flowchart of the segment fitting algorithm. We have made the code available at the Community Surface Dynamics Modeling System website: http://csdms.colorado.edu/wiki/Model:Chi_analysis_tools.

4. Examples

[33] We illustrate the technique using three examples. The first example uses topography generated from the Channel-Hillslope Integrated Landscape Development (CHILD) model [Tucker *et al.*, 2001]. This allows us to test whether the technique can identify known segments and retrieve a known m/n ratio. The next two examples are from natural landscapes. The first is from the Appalachian Plateau in Pennsylvania, U.S., where the combination of relatively homogenous sandstone bedrock and tectonic quiescence is thought to result in steadily eroding channels [Hack, 1960].

The second is from a landscape in the Apennines in Italy that has been subject to a previously constrained change in tectonic uplift rate [e.g., Whittaker *et al.*, 2008].

4.1. A Numerical Example: A Simulated Three-Stage Acceleration in Uplift

[34] Our first example deploys our chi analysis method on a landscape simulated with the CHILD landscape evolution model. We have chosen to run the method on a numerical simulation because it allows us to enforce equation (1) and to prescribe both the uplift history and m/n ratio. Our simulation involves three development stages. The model domain is a $6 \times 6 \text{ km}^2$ with an average node spacing of 50 m. Throughout the simulation, one boundary is set to a fixed elevation (defined as $z = 0 \text{ m}$), and the other boundaries are no flux boundaries. We use model parameters adapted from Attal *et al.*’s [2011] study of the evolution of catchments responding to tectonics in the Apennines using the CHILD model. Erosion is purely detachment limited: Erosion rates are calculated according to equation (1); furthermore, there is neither threshold for erosion nor adjustment in channel geometry [Attal *et al.*, 2011]. The parameters used in the model and the calculation of erosion rates are detailed in the Appendix A. The hillslope transport coefficient is set to $0.001 \text{ m}^2 \text{ yr}^{-1}$, channel erodibility (K) is set to $1.67 \times 10^{-6} \text{ yr}^{-1}$, m is set to 0.5 and n is set to 1 (Appendix A). In the first stage, a fixed uniform uplift rate of 0.3 mm yr^{-1} is prescribed. This uplift rate is maintained until the model domain achieves dynamic steady state, that is, erosion rates match the uplift rate of 0.3 mm yr^{-1} throughout the entire landscape. At this stage, rivers are characterized by smooth concave up river profiles. The uplift rate is then increased to 0.6 mm yr^{-1} for 1 Ma and then further increased to 0.9 mm yr^{-1} for a further 0.5 Ma. In response to the successive increases in uplift rate, steepened reaches develop upstream of the base level, separated from the upstream reaches by profile convexities that migrate upstream through time, representing the propagation of erosional waves that is diagnostic of detachment-limited systems [e.g., Whipple and Tucker, 1999; Attal *et al.*, 2011].

[35] The CHILD model runs on a triangulated irregular network (TIN), and channel profiles are extracted directly from the TIN. We use equation (1) to calculate erosion rates along the channels at the end of the run and find three sections with distinct erosion rates separated by transition zones (Figure 7a). We infer that these transition zones are present because CHILD uses an explicit numerical method (i.e., it uses model topographic parameters to calculate topographic changes at the following time step; Tucker *et al.* [2001]), which is susceptible to numerical dispersion [e.g., Fagherazzi *et al.*, 2002]. At the end of our simulation, the main stem river profile features two prominent convexities delineating three reaches (Figure 7b): upstream of the uppermost convexity, the river profile is adjusted to the initial uplift rate of 0.3 mm yr^{-1} and has not responded to any of the increases in uplift rate; between the two convexities, the river profile has adjusted to the uplift rate of 0.6 mm yr^{-1} ; downstream of the lowermost convexity, the steep reach is in equilibrium with the final uplift rate of 0.9 mm yr^{-1} . The two convexities are migrating upstream in concert at a celerity given by equation (5). Because $n = 1$ in the model, the celerity is independent of slope and thus of uplift rate so the convexities never meet, and the intermediate segment is

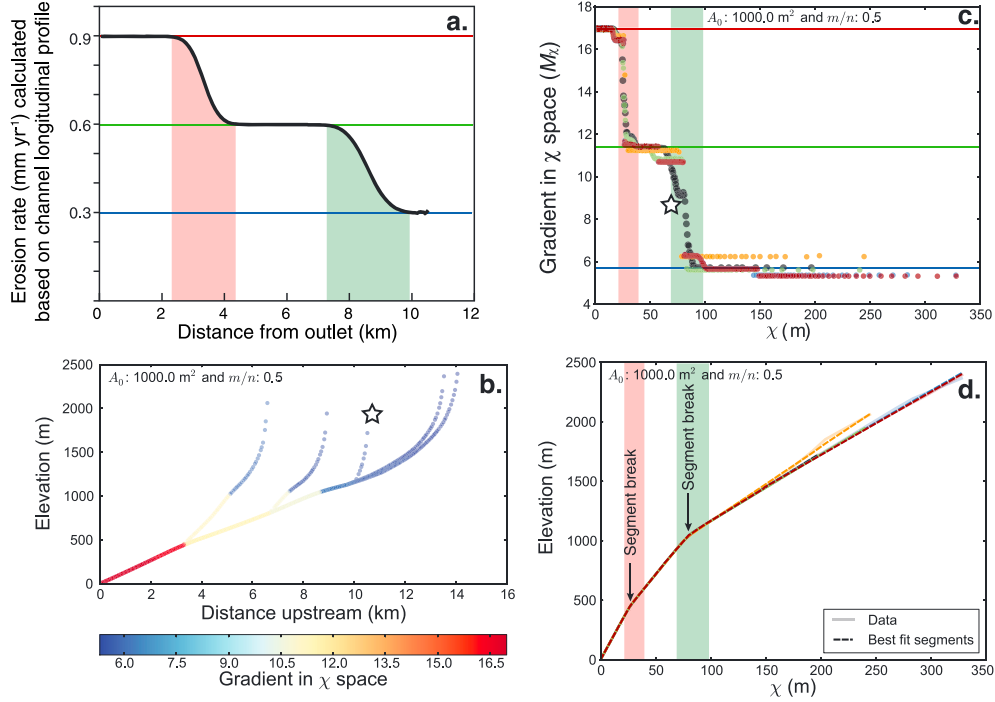


Figure 7. Results from CHILD model runs. (a) Erosion rates calculated along the channel (b, c) denoted by a star using equation (1), which is prescribed in the model. Figure 7b denotes channel longitudinal profiles colored by the extracted M_χ values. Figure 7c shows M_χ values as a function of χ ; each tributary is denoted by a different color. The tributary depicted in Figure 7a (star in Figure 7b) is plotted in black. (d) Chi plot of fitted and transformed data of all channels. In Figures 7a, 7c, and 7d the red- and green-shaded bars denote the transition zones between domains adjusted to the different phases of uplift. The horizontal red, green, and blue lines in Figure 7c represent the M_χ values corresponding to erosion rates of 0.9 mm yr⁻¹, 0.6 mm yr⁻¹, and 0.3 mm yr⁻¹, respectively, calculated using equation (6). Figures 7b–7d were generated with a mean skip value of 1, a minimum segment length of 12, 100 target nodes, and a σ value of 3 m.

preserved until the wave of erosion has propagated all the way to the top of the network.

[36] Results from segment extraction with the best fit m/n ratio of 0.5 (see next paragraph) demonstrate that the algorithm is able to detect the sections of the channel network responding to different uplift rates (Figures 7b–7d). In addition to being able to identify distinct channel segments, the algorithm is also able to retrieve M_χ values extremely close to the theoretical values predicted by equation (6) (Figure 7c).

[37] Our segment fitting algorithm is able to tightly constrain the most likely m/n ratio for these simulations. Figures 8a and 8b show that plausible values of the m/n ratio (those that have AICc values within 1 standard deviation of the m/n ratio with the minimum AICc value) clustered tightly around 0.5 (in Figures 8a and 8b, m/n ratios of 0.475–0.525 are considered plausible). The method correctly identifies the m/n ratio of 0.5 as the most likely.

4.1.1. Sensitivity Analysis and Recommended Default Parameters

[38] We performed a sensitivity analysis on the effect of changing the number of target nodes, the minimum segment length, the value of σ and the mean skip value using results from the CHILD simulations. We varied σ from 1 to 9 m, the mean skip value from 1 to 4, the minimum segment length from 6 to 20 nodes, and the number of target nodes from 60 to 100. Parameters generated similar results over a wide range of values for the main stem. The minimum

segment length and number of target nodes, however, can significantly alter computational time. Running the method on the CHILD data with target nodes = 100 and minimum segment length = 20 took a few minutes, whereas the run with target nodes = 100 and minimum segment length = 5 took 4 days on our Linux servers (i.e., 5–6 orders of magnitude longer). This strong dependence on computation time is due to the nonlinearity of the partition function. Sensitivity analysis shows that (i) increasing σ , the minimum segment length or the mean skip decreases the number of segments; (ii) one consequence of reducing the number of segments is that tributaries will be fit with single segment and information about changing steepness will be lost; and (iii) the number of target nodes can have a large influence on computational time but does not have a commensurate effect on the extracted segments. The least conclusive results were obtained when high values of mean skip (≥ 3) or minimum segment length were used.

[39] In every analysis performed by the method on the CHILD model runs, the most likely m/n ratio has been calculated as 0.5. The best fit m/n ratio has similarly returned 0.5 as the most likely m/n ratio for all individual channels except in the cases where minimum segment length or mean skip parameters have resulted in < 3 segments, which only occurred in the shortest tributaries.

[40] Our sensitivity analyses on the CHILD runs and in other landscapes have helped us develop some qualitative rules of thumb for selecting parameter values. We suggest

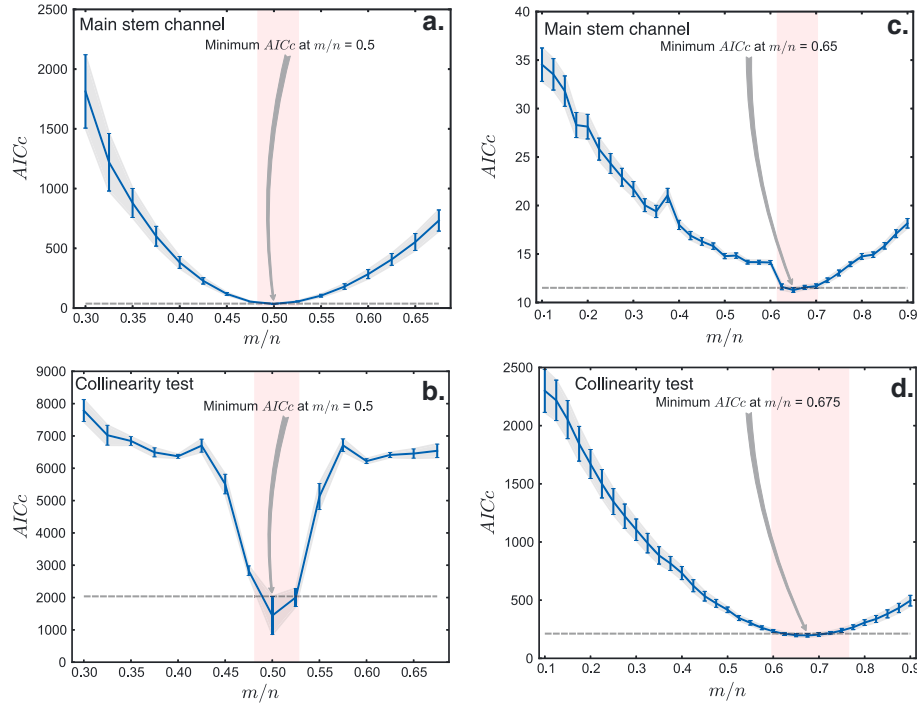


Figure 8. Plot of AICc values as a function of m/n ratio for CHILD model runs for (a) the main stem channel and (b) the collinearity test, and for Fonner Run, PA, for (c) the main stem and (d) the collinearity test. Errors represent 1 standard deviation of the AICc value measured after 250 iterations of the segment finding algorithm. Dashed line indicates the minimum AICc value plus 1 standard deviation. Red box shows range of m/n values where the AICc value is within 1 standard deviation of the minimum AICc value. Parameter values are for CHILD runs, mean skip value = 1, minimum segment length = 12, number of target nodes = 100, and $\sigma = 3$ m; for Fonner Run, mean skip value = 2, minimum segment length = 15, number of target nodes = 100, and $\sigma = 3$ m.

minimum segment lengths of 10–15 and a number of target nodes of 80–100. Increasing the number of target nodes does not seem to alter results substantially and results in very long compute times. Standard deviation of elevations (σ) and the skip value should be selected based on the resolution and quality of the digital elevation model (DEM). For 30 to 90 m resolution DEMs, we suggest skip values of 0–2 and σ values on the order of tens of meters. Ten meter resolution DEMs should have skip values of 1 to 4 and a σ similar to the reported uncertainty in elevation data, with some additional uncertainty due to topographic “noise” (i.e., boulders in channels). For 1 to 2 m resolution data, skip values of 5–10 will be more appropriate, and σ will most likely be on the order of meters. These parameters can be used to rapidly identify segments in a channel network; however, natural channels are not all as well behaved as simulated channels (see section 4.3) so we suggest that a sensitivity analysis is conducted as part of any analysis of channel steepness.

4.2. Fonner Run in Southwest Pennsylvania, U.S.

[41] Our second example comes from the western flank of the Appalachians in southwest Pennsylvania. We have selected a small basin called Fonner Run at 39.969391°N, 80.254147°W, for analysis (Figure 9a). This basin is in the same tectonic and geologic setting as Rush Run, which was analyzed by *Perron and Royden* [2013], but lies ~140 km to the northeast. Rivers here flow through a dendritic channel network over sandstone bedrock [*Miles and Whitfield*, 2001].

The site is tectonically quiescent and is to the south of the southernmost extent of Quaternary glaciations [*Peltier*, 2004].

[42] Our method finds a best fit m/n ratio of 0.675 based on the collinearity test, whereas the best fit m/n ratio of the main stem channel is 0.65 (Figures 8c and 8d). Plots of AICc as a function of m/n ratio at this site indicate that plausible values (i.e., those within 1 standard deviation of the minimum AICc, in this case after 250 iterations of the segment finding algorithm) for the m/n ratio range from 0.6 to 0.7 (Figures 8c and 8d). For Rush Run, *Perron and Royden* [2013] found that, qualitatively, an m/n value of 0.65 best collapses the tributaries. They note that this m/n ratio leads to a convex up main stem channel. Our analysis of Fonner Run yields qualitatively the same result: the m/n ratio that best collapses the tributaries (as determined in our case by the collinearity test) leads to a main stem that appears slightly convex (Figure 9). However, our segment fitting algorithm finds that the m/n ratio that best describes the main stem channel as a series of linear segments is similar to the best fit m/n ratio for collinearity. Because the two analyses yield similar results, we can have some confidence that the main stem channel does in fact have different segments, and the apparent convexity is not simply a by-product of selecting an inappropriate m/n ratio. Our segment fitting algorithm finds that the best explanation for the channel profile is one made up of two segments, with the downstream segment having a slightly greater value of M_x (Figure 9). This downstream steepening may have multiple causes, including changes in

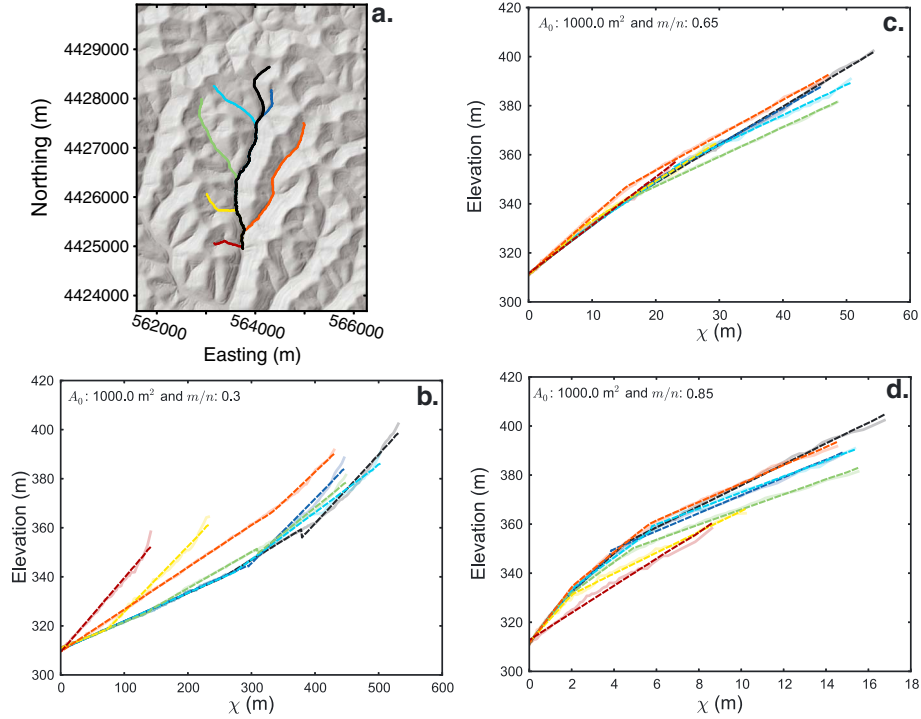


Figure 9. (a) Fonner Run network over a hillshade map, UTM zone 17N. Plots of the χ -elevation profiles for m/n ratios of (b) 0.3, (c) 0.65, and (d) 0.8. The dashed lines are the best fit segments, and the solid lines are the transformed data. Parameter values are the same as in Figure 8. An m/n ratio of ~ 0.65 gives the best fit for both main stem profile and collinearity test.

the rate of base level lowering, a subtle change in rock resistance to erosion or a nonuniform rainfall pattern causing a breakdown of the relationship between drainage area and discharge. In this case, the study catchment is of a small enough scale that nonuniform precipitation is unlikely, so the steepened lowermost reach is probably caused either by harder sedimentary layers downstream or by an incision signal that has propagated up from the Ohio River, which has incised during the Pleistocene [e.g., *Granger et al.*, 2001]. Figure 9 shows that m/n ratios outside of the range of plausible m/n ratios produce chi plots that do not have collinear tributary channels.

4.3. Rio Torto, Apennines, Italy

[43] Our third example is from a tectonically active area in the Apennines of central Italy. The study catchment is bounded by the Fiamignano Fault, a normal fault that has seen an increase in throw rate from 0.3 to 1.0 mm yr⁻¹ approximately 0.75 Ma ago [Roberts and Michetti, 2004; Whittaker et al., 2008; Attal et al., 2011]. Royden and Perron [2013] examined one of the tributaries within this catchment. They fixed $m/n=0.4$ and fit analytical solutions to the measured profile using scenarios in which uplift occurred in two stages. From this, Royden and Perron [2013] inferred that $n=0.5$ on the basis that the relative steepness of two distinct segments in the chi plot was consistent with the known difference in uplift rates.

[44] We performed segment fitting analysis on a network of the main stem Rio Torto (as determined by flow distance) and four tributaries upstream of the Fiamignano Fault (Figure 10). The best fit m/n ratio in the Rio Torto Basin is poorly constrained compared to both CHILD model runs and the Fonner Run. We compiled the most likely m/n ratio across a

range of parameter values: we varied mean skip between 1 and 3, minimum segment length between 8 and 20, the number of target nodes between 60 and 150, and set σ to 20 m because our fieldwork has shown that the DEM occasionally misses the floor of the gorges resulting in large error on the order of 20 m. The result of this analysis is shown in Figure 11. The collinearity test does not provide tight constraints on the most likely m/n ratio due to the presence of a tributary that appears to hang above the rest of the tributary network (tributary 4, Figures 10a and 10c). The main stem channel also is poorly constrained, with the 25th to 75th percentile of most likely m/n ratios spanning 0.15 to just over 0.6, again due to the existence of multiple convexities. Tributaries 1, 2, and 3 give the tightest constraints on the m/n ratio, but these estimates of the most likely m/n ratio strongly differ. Such uncertainty is perhaps to be expected in locations with such tectonic, lithologic, and structural complexity as the central Apennines. These results highlight the need to explore and report our method's parameter space when selecting the m/n ratio.

[45] Regardless of the m/n ratio, profiles in χ -elevation space all indicate a steepened reach upstream of the fault, consistent with the known increase in relative uplift rate experienced by the catchment [Whittaker et al., 2008; Attal et al., 2011], as well as additional steepened reaches in the headwaters of the main stem and tributary 4 (Figure 10). This headwater steepening corresponds to lithological changes associated with post-Miocene faults [ISPRA, 2010] that show no sign of recent (i.e., Holocene) activity in the field [Roberts and Michetti, 2004]. This example highlights the way the method can be used to identify locations that merit further field investigation.

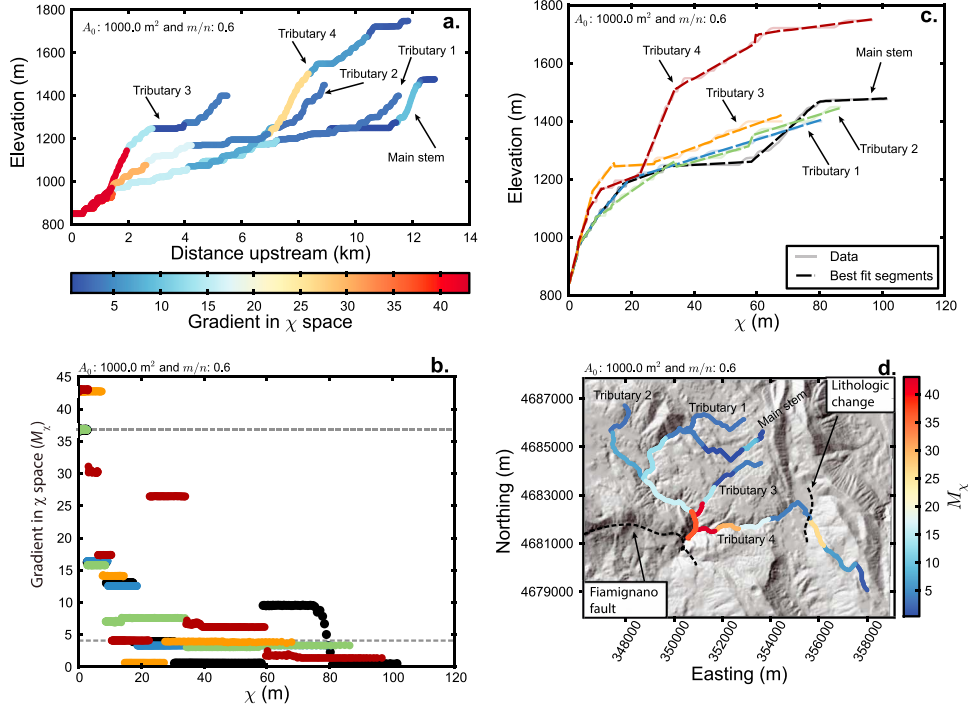


Figure 10. Results of segment fitting algorithm for the Rio Torto and tributaries using an m/n ratio of 0.6. Parameter values are mean skip = 1, number of target nodes = 100, minimum segment length = 12, and $\sigma = 20$ m. (a) Channel profiles colored by the best fit M_χ . (b) Calculated values of M_χ for each tributary. Dashed gray lines denote segments selected to calculate M_χ ratio. (c) Best fit segments (dashed lines) and transformed data (solid lines) in χ -elevation space. (d) Map of Rio Torto projected in UTM zone 33N; the outlet of the study catchment is at approximately 42.267655°W, 13.186485°E. Channels colored by best fit M_χ shown on a hillshade of the study catchment.

4.3.1. Using M_χ to Constrain the n Exponent in Locations With Known Uplift Rates

[46] Royden and Perron [2013] asserted that in rivers with similar precipitation and erodibility but different uplift rates, the ratio between M_χ values is proportional to the ratio between uplift rates raised to the $1/n$ power. Here we explore this assertion, which can be used to determine the n exponent, and extend it to cases where erodibility is a function of uplift rate, as suggested by some authors [e.g., Snyder *et al.*, 2003]. In segments unaffected by stretch zones, M_χ is related to erosion rate, erodibility and other parameters according to equation (6). Assuming that segments represent stretches of the river equilibrated to the uplift rate that led to their formation, uplift rate can be substituted for erosion rate, and equation (6) can be rearranged as follows:

$$M_\chi^n K A_0^m = U. \quad (10)$$

[47] If we have two separate segments with separate values of M_χ we can relate these to a ratio between uplift rates:

$$\frac{M_{\chi,1}^n K A_0^m}{M_{\chi,2}^n K A_0^m} = \frac{U_1}{U_2}. \quad (11)$$

[48] Again, this equation assumes that there has been some equilibration between uplift and erosion rate or, in other words, that uplift has been sustained for long enough to be

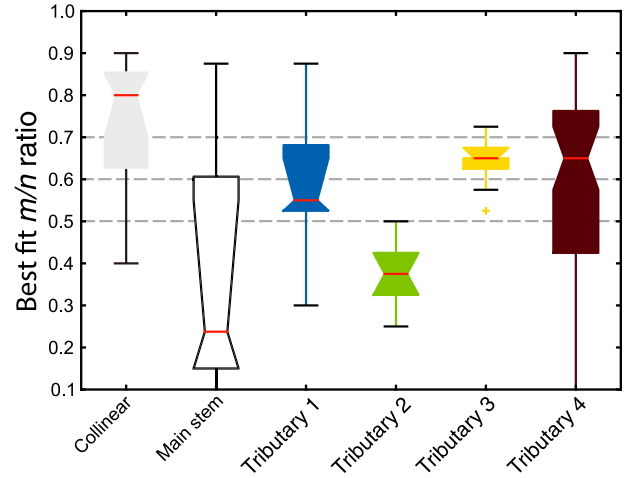


Figure 11. Box-and-whisker plot of the best fit m/n ratio for the Rio Torto channel network. The red lines are the median most likely m/n ratios across 30 parameter values (varying skip, minimum segment length, and number of target nodes). The whiskers are the data range (with one outlier in channel 3), the boxes extend between the 25th and 75th percentiles of the data, the tapering extends to the 95% confidence intervals of the median most likely m/n ratio calculated by bootstrapping the data 10,000 times. Dashed lines inserted as a visual aid to identify m/n ratios of 0.5, 0.6, and 0.7.

reflected in the channel profile. Therefore, estimates of erosion rates or uplift rates that represent timescales of thousands to millions of years would be appropriate for such an analysis, whereas measurements of suspended sediment, which vary on interannual timescales, may not capture the full range of erosion rates that drive topographic signatures of uplift rates. The parameter A_0 is a constant, and if we assume K is a constant, equation (11) simplifies to

$$\left(\frac{M_{\chi,1}}{M_{\chi,2}}\right)^n = \frac{U_1}{U_2}. \quad (12)$$

[49] The ratio of uplifts is thus equal to the ratio of M_χ to the power n .

[50] Some authors have suggested that the erodibility of bedrock channels is a function of uplift rates. If we assume the erodibility coefficient has the form $K = kU^a$ [e.g., *Snyder et al.*, 2003; *DiBiase et al.*, 2010], then equation (12) can be recast as

$$\left(\frac{M_{\chi,1}}{M_{\chi,2}}\right)^{ne} = \frac{U_1}{U_2}, \quad (13)$$

where ne is an “effective” slope exponent where $ne = n/(1 - a)$. If we solve equation (12) for the slope exponent n (and note that equation (13) has the same form as equation (12) so can similarly be solved for ne), we find that

$$n = \text{Log} \left[\frac{U_1}{U_2} \right] / \text{Log} \left[\left(\frac{M_{\chi,1}}{M_{\chi,2}} \right) \right]. \quad (14)$$

[51] In practice, one can only use equation (14) if the m/n ratio is constrained beforehand, since the m/n ratio affects the values of M_χ derived for each segment and thus the M_χ ratio. In the Rio Torto, we follow *Attal et al.* [2011] and assume the upstream segments are equilibrated to a fault throw rate of $\sim 0.3 \text{ mm yr}^{-1}$ whereas the downstream segments are equilibrated to a fault throw rate of $\sim 1.0 \text{ mm yr}^{-1}$. These rates yield an uplift ratio of ~ 3.3 . Regardless of parameter combinations, the transformed channels are composed of several distinct segments. We use the average value of M_χ from tributaries 1, 2, and 3 to calculate M_χ ratios since these channels appear to have the most consistent profiles (Figures 10b and 10c). We use the most downstream segment on each of these channels, which is bounded by the fault, and the segments in these channel that sit on the plateau.

[52] Using these criteria leads to M_χ ratios of ~ 4.3 , 8, and 10, respectively when the most likely m/n ratios are 0.5, 0.6, and 0.7, respectively (Figure 11). These M_χ ratios result in an estimate of n between 0.52 and 0.82, that is, at the lower end of the range of values suggested based on a physical description of the erosion processes at work in bedrock rivers [*Whipple et al.*, 2000]. Note however that in addition to the lithological variations mentioned in section 4.3, the complexity of the tectonic setting in the Apennines may also lead to difficulties when trying to invert topographic data to retrieve stream power parameters: for example, the Rio Torto basin is experiencing back-tilting as it is being uplifted [e.g., *Attal et al.*, 2011], potentially causing a reduction in the steepness of the upstream

reaches which may lead to an anomalously high M_χ ratio (and thus a low n estimate).

5. Conclusions

[53] We present a method for analyzing channel longitudinal profiles in order to extract information about erodibility or erosion rates. Our method extracts the most statistically likely channel segments that have distinct steepness, normalized for drainage area through the integral method of channel profile analysis. This method eliminates the need for initial processing of the raw topographic data (e.g., smoothing of river profiles to derive channel slope) which inevitably leads to loss of information. In locations where the stream power incision model can predict channel incision rates, our method can be used to quantify the most likely m/n ratio and locate channel segments with distinct erosion rates or erodibilities (where erodibility refers to the K parameter in the stream power law, which encapsulates the influence of bedrock strength, climate, sediment supply, erosion thresholds, and channel width adjustment on the susceptibility of bedrock to fluvial erosion). The method also reports uncertainties in the most likely m/n ratio. Our tests on an idealized, simulated landscape and on a landscape on the Appalachian Plateau resulted in tightly constrained m/n ratios and identification of distinct segments within the fluvial networks. In the case of the modeled landscape, these distinct segments predictably reflect the changes in uplift rate applied during the simulation. In a tectonically and structurally complex landscape in the Apennines in Italy, the uncertainty on the estimates of m/n ratio is much greater but the segments identified are nevertheless consistent with the known tectonic history of the area. We also show how users may apply our method to quantify the n exponent in locations where erosion rates are well constrained.

6. Author Contributions

[54] S.M.M. designed the algorithms. S.M.M., D.T.M., and S.W.D.G. wrote the code. M.A. performed CHILD simulations. S.M.M., D.T.M., S.W.D.G., and D.A.V. wrote visualization scripts, and S.M.M., M.A., D.T.M., S.W.D.G., and D.A.V. performed the analyses and wrote the paper.

7. Software Availability

[55] Source code, documentation, instructions, and channel profile data are available via the Community Surface Dynamics Modeling System at http://csdms.colorado.edu/wiki/Model:Chi_analysis_tools.

Appendix A: Description of the Calculation of Erosion Rates in the CHILD Model

[56] In the CHILD model, erosion rates are calculated using equations that can be combined to give equation (1) [see *Tucker et al.*, 2001; *Attal et al.*, 2011]. Simulations presented here are for a scenario in which erosion is purely detachment limited, and there are neither erosion thresholds nor adjustment in channel geometry [cf. *Attal et al.*, 2008, 2011]. First, the model calculates potential hillslope and fluvial erosion rates according to equations (A1) and (A2), respectively (see below). Erosion driven by soil creep is computed

based on the divergence of volumetric sediment discharge per unit width q_c , which is calculated with

$$q_c = -K_d \nabla z, \quad (\text{A1})$$

where K_d [$\text{L}^2 \text{T}^{-1}$] is a hillslope transport coefficient and z [L] is surface elevation. Fluvial erosion rate E [L T^{-1}] is calculated following:

$$E = k_b \tau^{pb}, \quad (\text{A2})$$

where k_b is a specific bedrock erodibility coefficient (in L T^{-1} per “stress quantity” in SI units), τ [$\text{M L}^{-1} \text{T}^{-2}$] is fluvial shear stress, and pb is a dimensionless constant. The erosion rate calculated by both equations is compared, and the elevation of the node is lowered by the largest amount predicted by either of the two equations. Beyond a given drainage area, fluvial processes become dominant, and equation (A2) prevails. The shear stress quantity (the unit of which depends on the values chosen for exponents mb and nb) is calculated according to

$$\tau = k_t (Q/W)^{mb} S^{nb}, \quad (\text{A3})$$

where Q is water discharge [$\text{L}^3 \text{T}^{-1}$], W [L] is channel width, k_t is a scaling parameter, and mb and nb are constants. Here, channel width is calculated using the simplest form of hydraulic scaling available in CHILD [Leopold and Maddock, 1953]:

$$W = k_w Q^{1/2}, \quad (\text{A4})$$

where k_w is a hydraulic scaling coefficient [$\text{L}^{-1/2} \text{T}^{1/2}$]. In the model, we assume no infiltration so that discharge is only the product of the precipitation rate P in [L T^{-1}] by drainage area:

$$Q = PA. \quad (\text{A5})$$

[57] Combining equations (A2) to (A5) gives

$$E = k_b k_t^{pb} k_w^{(-pb \cdot mb)} P^{(pb \cdot mb/2)} A^{(pb \cdot mb/2)} S^{(pb \cdot nb)}. \quad (\text{A6})$$

[58] This equation is equivalent to equation (1), with $m = pb \cdot mb/2$, $n = pb \cdot nb$, and $K = k_b k_t^{pb} k_w^{(-pb \cdot mb)} P^{(pb \cdot mb/2)}$. Note that the exponents mb , nb , and pb can be set to simulate different fluvial incision laws (i.e., incision rate proportional to fluvial shear stress, cross-section-averaged stream power or specific stream power). In our example, we assume that erosion rate is proportional to stream power per unit bed area (so-called specific stream power) and set $mb = nb = pb = 1$. Equation (A6) thus becomes

$$E = KA^{1/2} S \quad (\text{A7})$$

with $K = k_b k_t k_w^{-1} P^{1/2}$ [T^{-1}]. We thus have $m = 0.5$, $n = 1$, and $m/n = 0.5$. In this case, the quantity τ in equation (A3) represents the specific stream power [M T^{-3}], and k_t is the specific weight of water ($9810 \text{ kg m}^{-2} \text{s}^{-2}$ in SI units). The value of k_b has to be adjusted with respect to Attal *et al.*'s [2011] study where the exponents were set to different values ($mb = 0.6$, $nb = 0.7$, and $pb = 1.5$): in the present study, we set $k_b = 2.2 \times 10^{-5} \text{ m yr}^{-1} (\text{W m}^{-2})^{-1}$ as the equivalent of the value of $5.2 \cdot 10^{-6} \text{ m yr}^{-1} \text{ Pa}^{-3/2}$ that was used in Attal *et al.* [2011]. We use $k_w = 4.6 \text{ m}^{-1/2} \text{s}^{1/2}$ to

replicate the hydraulic scaling relationship without adjustment in channel geometry constrained in the Apennines [Attal *et al.*, 2008]. We use rainfall parameters identical to those in Attal *et al.* [2011], except that we do not allow the parameters to vary around their mean value during the runs; the CHILD model produces storms according to a Poisson rectangular pulse rainfall model [Tucker and Bras, 2000], using the following values: mean precipitation rate = 0.75 mm/h, mean storm duration = 22 h, and mean interstorm duration = 260 h. This means that each year, it rains 7.8% of the time at a rate of 0.75 mm/h, thus equivalent to an average yearly rainfall $P = 1.63 \cdot 10^{-8} \text{ m s}^{-1}$. We thus derive $K = 1.67 \cdot 10^{-6} \text{ yr}^{-1}$ (equation (A7)).

[59] **Acknowledgments.** We thank Jen Merritt, Fiona Clubb, Amy Ball, Rahul Devrani, Vimal Singh, Martin Hurst, and T.C. Hales for beta testing the software. Greg Tucker provided advice on CHILD simulations, and we thank Taylor Perron, Sean Gallen, Alex Densmore, and an anonymous referee for their comments and suggestions. This work was supported by the Carnegie Trust for the Universities of Scotland and NERC grant NE/J012750/1 to Mudd. David Milodowski is supported by NERC grant NE/J500021/1, and Stuart Grieve is supported by NERC grant NE/J009970/1.

References

- Akaike, H. (1974), A new look at the statistical model identification, *IEEE Trans. Autom. Control*, 19(6), 716–723, doi:10.1109/TAC.1974.1100705.
- Andrews, G. E. (1998), *The Theory of Partitions*, England, Cambridge Univ. Press, Cambridge.
- Attal, M., G. E. Tucker, A. C. Whittaker, P. A. Cowie, and G. P. Roberts (2008), Modeling fluvial incision and transient landscape evolution: Influence of dynamic channel adjustment, *J. Geophys. Res.*, 113, F03013, doi:10.1029/2007JF000893.
- Attal, M., P. A. Cowie, A. C. Whittaker, D. Hobley, G. E. Tucker, and G. P. Roberts (2011), Testing fluvial erosion models using the transient response of bedrock rivers to tectonic forcing in the Apennines, Italy, *J. Geophys. Res.*, 116, F02005, doi:10.1029/2010JF001875.
- Burnham, K. P., and D. R. Anderson (2002), *Model Selection and Multimodel Inference: A Practical Information-Theoretic Approach*, 2nd ed., 488 pp., Springer-Verlag, New York, ISBN:0-387-95364-7.
- Cowie, P. A., A. C. Whittaker, M. Attal, G. P. Roberts, G. E. Tucker, and A. Ganas (2008), New constraints on sediment-flux-dependent river incision: Implications for extracting tectonic signals from river profiles, *Geology*, 36, 535–538, doi:10.1130/G24681A.1.
- Davis, W. M. (1899), The geographical cycle, *Geogr. J.*, 14(5), 481–504.
- DiBiase, R. A., K. X. Whipple, A. M. Heimsath, and W. B. Ouimet (2010), Landscape form and millennial erosion rates in the San Gabriel Mountains, CA, *Earth Planet. Sci. Lett.*, 289, 134–144, doi:10.1016/j.epsl.2009.10.036.
- Eckert, S., T. Kellenberger, and K. Itten (2005), Accuracy assessment of automatically derived digital elevation models from ASTER data in mountainous terrain, *Int. J. Remote Sens.*, 26(9), 1943–1957, doi:10.1080/0143116042000298306.
- Fagherazzi, S., A. D. Howard, and P. L. Wiberg (2002), An implicit finite difference method for drainage basin evolution, *Water Resour. Res.*, 38(7), 116, doi:10.1029/2001WR000721.
- Granger, D. E., D. Fabel, and A. N. Palmer (2001), Pliocene-Pleistocene incision of the Green River, Kentucky, determined from radioactive decay of cosmogenic ^{26}Al and ^{10}Be in Mammoth Cave sediments, *Geol. Soc. Am. Bull.*, 113(7), 825–836, doi:10.1130/0016-7606(2001)113%3C0825:PPIOTG%3E2.0.CO;2.
- Hack, J. T. (1960), Interpretation of erosional topography in humid temperate regions, *Am. J. Sci.*, 258-A, 80–97.
- Hansen, M. H., and C. Kooperberg (2002), Spline adaptation in extended linear models, *Stat. Sci.*, 17(1), 2–51, doi:10.1214/ss/1023798997.
- Harkins N., E. Kirby, A. Heimsath, R. Robinson, and U. Reiser (2007), Transient fluvial incision in the headwaters of the Yellow River, northeastern Tibet, China, *J. Geophys. Res.*, 112, F03S04, doi:10.1029/2006JF000570.
- Hobley, D. E. J., H. D. Sinclair, S. M. Mudd, and P. A. Cowie (2011), Field calibration of sediment flux dependent river incision, *J. Geophys. Res.*, 116, F04017, doi: 10.1029/2010JF001935.
- Hodgson, M. E., and P. Bresnahan (2004), Accuracy of airborne lidar-derived elevation: Empirical assessment and error budget, *Photogramm. Eng. Remote Sens.*, 70(3), 331–339.
- Howard, A. D. (1994), A detachment-limited model of drainage basin evolution, *Water Resour. Res.*, 30, 2261–2285.

- Howard, A. D., and G. Kerby (1983), Channel changes in badlands, *Bull. Geol. Soc. Am.*, 94(6), 739–752.
- Hurvich, C. M., and C.-L. Tsai (1989), Regression and time series model selection in small samples, *Biometrika*, 76, 297–307.
- ISPRA (2010), Carta geologica d'Italia, Foglia 658: Pescorocchiano (1:50,000), Servizio Geologico d'Italia.
- Kirby, E., and W. Ouimet (2011), Tectonic geomorphology along the eastern margin of Tibet: Insights into the pattern and processes of active deformation adjacent to the Sichuan Basin, *Geol. Soc. Lond. Spec. Publ.*, 353, 165–188, doi:10.1144/SP353.9.
- Kirby, E., and K. X. Whipple (2001), Quantifying differential rock-uplift rates via stream profile analysis, *Geology*, 29, 415–418.
- Kirby, E., and K. X. Whipple (2012), Expression of active tectonics in erosional landscapes, *J. Struct. Geol.*, 44(0), 54–75, doi:10.1016/j.jsg.2012.07.009.
- Kirby, E., K. X. Whipple, W. Q. Tang, and Z. L. Chen (2003), Distribution of active rock uplift along the eastern margin of the Tibetan Plateau: Inferences from bedrock channel longitudinal profiles, *J. Geophys. Res.*, 108, 2217, doi:10.1029/2001JB000861.
- Lague D. (2010), Reduction of long-term bedrock incision efficiency by short-term alluvial cover intermittency, *J. Geophys. Res.*, 115, F02011, doi:10.1029/2008JF001210.
- Lague, D. (2013), The stream power river incision model: Evidence, theory and beyond, *Earth Surf. Processes Landforms*, doi:10.1002/esp.3462, in press.
- Leopold, L. B., and T. Maddock (1953), The hydraulic geometry of stream channels and some physiographic implications, *USGS Prof. Paper*, 252.
- Miles, C. E., and T. G. Whitfield, compilers (2001), Bedrock geology of Pennsylvania, Pennsylvania Geological Survey, 4th ser., dataset, scale 1:250,000.
- Miller, S. R., R. L. Slingerland, and E. Kirby (2007), Characteristics of steady-state fluvial topography above fault-bend folds, *J. Geophys. Res.*, 112, F04004, doi:10.1029/2007JF000772.
- Peltier, W. R. (2004), Global glacial isostasy and the surface of the ice-age earth: The ICE-5G (VM2) model and GRACE, *Annu. Rev. Earth Planet. Sci.*, 32, 111–149, doi:10.1146/annurev.earth.32.082503.144359.
- Perron, J. T., and L. Royden (2013), An integral approach to bedrock river profile analysis, *Earth Surf. Processes Landforms*, 38, 570–576, doi:10.1002/esp.3302.
- Pritchard, D., G. G. Roberts, N. J. White, and C. N. Richardson (2009), Uplift histories from river profiles, *Geophys. Res. Lett.*, 36, L24301, doi:10.1029/2009GL040928.
- Roberts, G. P., and A. M. Michetti (2004), Spatial and temporal variations in growth rates along active normal fault systems: An example from Lazio-Abruzzo, central Italy, *J. Struct. Geol.*, 26, 339–376.
- Rosenbloom, N. A., and R. S. Anderson (1994), Evolution of the marine terraced landscape, Santa Cruz, California, *J. Geophys. Res.*, 99, 14,013–14,030.
- Royden, L., and J. T. Perron (2013), Solutions of the stream power equation and application to the evolution of river longitudinal profiles, *J. Geophys. Res. Earth Surf.*, 118, 497–518, doi:10.1002/jgrf.20031.
- Royden L. H., M. K. Clark, and K. X. Whipple (2000), Evolution of river elevation profiles by bedrock incision: Analytical solutions for transient river profiles related to changing uplift and precipitation rates, *EOS, Transactions of the American Geophysical Union*, 81, Fall Meeting Supplement, Abstract T62F-09.
- Seidl, M. A., and W. E. Dietrich (1992), The problem of channel erosion into bedrock, *Catena Suppl.*, 23, 101–124.
- Skiena, S. (1990), *Implementing Discrete Mathematics: Combinatorics and Graph Theory with Mathematica*, MA, Addison-Wesley, Reading.
- Sklar, L. S., and W. E. Dietrich (2004), A mechanistic model for river incision into bedrock by saltating bedload, *Water Resour. Res.*, 40, W06301, doi:10.1029/2003WR002496.
- Snyder, N. P., K. X. Whipple, G. E. Tucker, and D. J. Merritts (2003), Channel response to tectonic forcing: Field analysis of stream morphology and hydrology in the Mendocino triple junction region, northern California, *Geomorphology*, 53, 97–127.
- Stock, J. D., and D. R. Montgomery (1999), Geologic constraints on bedrock river incision using the stream power law, *J. Geophys. Res.*, 104(B3), 4983–4994.
- Tucker, G. E., and R. L. Bras (2000), A stochastic approach to modeling the role of rainfall variability in drainage basin evolution, *Water Resour. Res.*, 36(7), 1953–1964, doi:10.1029/2000WR900065.
- Tucker, G. E., and K. X. Whipple (2002), Topographic outcomes predicted by stream erosion models: Sensitivity analysis and intermodel comparison, *J. Geophys. Res.*, 107(B9), 2179, doi:10.1029/2001JB000162.
- Tucker, G. E., S. T. Lancaster, N. M. Gasparini, R. L. Bras, and S. M. Rybczyk (2001), An object-oriented framework for hydrologic and geomorphic modeling using triangulated irregular networks, *Comput. Geosci.*, 27(8), 959–973.
- Weissel, J. K., and M. A. Seidl (1998), Inland propagation of erosional escarpments and river profile evolution across the Southeast Australian passive continental margin, in *Rivers Over Rock: Fluvial Processes in Bedrock Channels*, Geophysical Monograph, vol. 107, edited by K. J. Tinkler and E. E. Wohl, pp. 189–206, AGU, Washington, D. C.
- Whipple, K. X., and G. E. Tucker (1999), Dynamics of the stream-power river incision model: Implications for height limits of mountain ranges, landscape response timescales, and research needs, *J. Geophys. Res.*, 104(B8), 17,661–17,674.
- Whipple, K. X., G. S. Hancock, and R. S. Anderson (2000), River incision into bedrock: Mechanics and relative efficacy of plucking, abrasion and cavitation, *Geol. Soc. Am. Bull.*, 112, 490–503, doi:10.1130/0016-7606(2000)112<490:RIIBMA>2.0.CO;2.
- Whittaker, A. C., M. Attal, P. A. Cowie, G. E. Tucker, and G. P. Roberts (2008), Decoding temporal and spatial patterns of fault uplift using transient river long-profiles, *Geomorphology*, 100, 506–526, doi:10.1016/j.geomorph.2008.01.018.
- Wobus, C., K. X. Whipple, E. Kirby, N. Snyder, J. Johnson, K. Spyropolou, B. Crosby, and D. Sheehan (2006), Tectonics from topography: Procedures, promise, and pitfalls, in *Tectonics, Climate, and Landscape Evolution*, Geological Society of America Special Paper, 398, Penrose Conference Series, edited by S. D. Willett et al., pp. 55–74, Geological Society of America, Boulder, CO.